Acta Acustica united with Acustica
Vol. 102 (2016) 1 – 1

A Plane and Thin Panel with Representative Simply Supported Boundary Conditions for Laboratory Vibroacoustic Tests

Olivier Robin[1)], Jean-Daniel Chazot[2)], Romain Boulandet[1)], Marc Michau[1)], Alain Berry[1)], Noureddine Atalla[1)]

[1)] Groupe d'Acoustique de l'Université de Sherbrooke, Faculté de génie mécanique, 2500 Boulevard de l'Université, Sherbrooke, QC, J1K2R1, Canada. olivier.robin@usherbrooke.ca

[2)] Sorbonne universités, Université de technologie de Compiègne, CNRS, Laboratoire Roberval UMR 7337, 60203 Compiègne Cedex, France

Summary

A technique to setup a simply supported rectangular plane panel for laboratory vibroacoustic tests is described and validated. For a given panel fixed to thin vertical supports, a dimensionless parameter is proposed to size these supports following a desired frequency precision compared to theoretical eigenfrequencies of a panel with such boundary conditions. A numerical study confirms the potential of this design parameter. Detailed instructions for assembling a panel with adequate thin vertical supports on a rigid frame are then given. Finally, three laboratory cases are described which illustrate possible experimental vibroacoustic applications using a panel assembled following previous guidelines. The design parameter viability is experimentally confirmed, and all obtained results depicted good agreement with analytical solutions and numerical predictions.

PACS no. 43.40.At, 43.40.Dx, 43.40.Vn

1. Introduction

In an article published in 1973 concerning the free vibration of rectangular plates, Leissa [1] pointed out that the book he had published years ago [2] yet showed the vast literature that concerned the free vibrations of rectangular plates (that was *'164 pertinent references'*, even when excluding *'such complicating effects as orthotropy, in-plane forces, variable thickness, the effects of surrounding media, large deflections, shear deformation and rotary inertia, and nonhomogeneity'*). When considering all possible combinations of classical boundary conditions (*i.e.* free, clamped, or simply-supported), 21 distinct cases exist for rectangular plates [1]. The boundary conditions of a vibrating plate together with their possible arrangements have a large influence on the plate vibration and sound radiation, and the specific case of finite simply supported plates is used as a core problem in several reference books (e.g. Williams [3], Fahy and Gardonio [4]) since such boundary conditions lead to a simple and exact analytical solution to the plate equation of motion.

Compared to numerous theoretical studies [2, 5], the problem of experimentally realizing plane panels with simply supported conditions has received very little attention, despite the interest of having access to a laboratory tool that would behave closely to an exact mathematical model. To the best of the authors knowledge, the only papers that explicitly aim at realizing a panel with simply supported boundary conditions for vibroacoustic testing, and report both experimental setup and test of such a panel were published by Ochs and Olson [6], Champoux *et al.* [7], Hoppmann and Greenspon [8], and Barnard and Hambric [9]. Note that a similar setup to the one of Ochs and Olson [6] is depicted in Hansen [10] (but no reference to a specific publication nor to an experimental validation was given), and nearly identical experime ntal implementations were reported by Pan *et al.* [11] and Yoon and Nelson [12]. The use of machined grooves proposed by Barnard and Hambric [9] was also suggested years ago by Hoppmann and Greenspon [8], but with V-shaped grooves. In most of these publications [6, 7, 8, 9, 12], the reported experimental validations were all satisfactory, with a good agreement between measured and calculated natural frequencies, mobility or mean quadratic velocity of the panel. Note that the problem of achieving accurate simply supported boundary conditions, apart the specific objective of vibroacoustic testing, has been also investigated for compression testing of uniaxially loaded panels as an example [13].

Illustrations of the suggested plate supports in [6, 7, 8, 9] are reprinted from the corresponding papers and given in Figures 1a-d, respectively. From the examples illustrated in Figures 1a,b, some technical limitations emerge: (1) screws mounting along the panel edges can be highly

Received 29 August 2015,
accepted 20 October 2015.

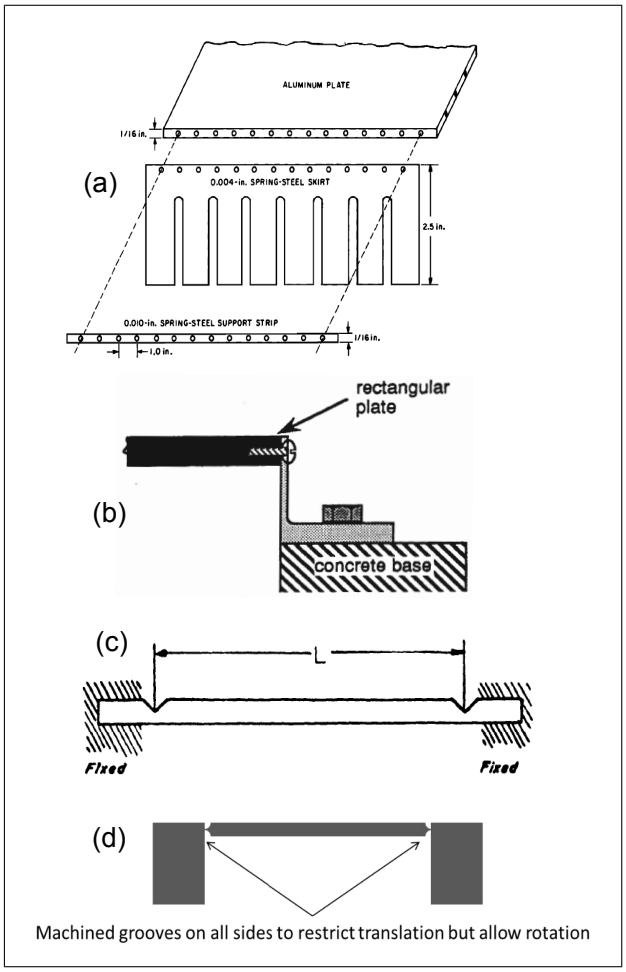

Figure 1. (a) Proposed and tested plate support in Ochs [6] [Reprinted with permission from J.B. Ochs and J.C. Snowdon, The Journal of the Acoustical Society of America, Vol. 58(4), pp.832-840 (1975). Copyright ©1975, American Institute of Physics] - (b) Proposed and tested plate support in Champoux [7] - (c) Proposed and tested plate support in Hoppmann [8] [Reprinted with permission from Hoppmann and Greenspon [8]. Copyright ©1954, American Society of Mechanical Engineers] - (d) Proposed and tested plate support in Barnard [9] [Reprinted with permission from Barnard and Hambric [9]. Copyright ©2014, Institute of Noise Control Engineering].

complex especially for small plate thicknesses (such as for the 1/16 in. thick plate in [6]), and (2) the mounting of the panel on a concrete base [7] makes its handling quite difficult. The machined grooves illustrated in Figure 1c,d might also be difficult to realize in practice and if ever broken can be hardly repaired (Hoppmann and Greenspon [8] suggested that the groove or notch depth should be at least eight-tenths times the panel thickness to correctly approach simply-suppor ted conditions, which is in good agreement with the 0.04 in. thick groove surrounding the 1/4 in. panel in [9]).

The main goal of this paper is to thoroughly describe a technique that allows realizing representative simply supported boundary conditions on a panel and obtaining a functional experimental mean that can easily adapt to typical vibroacoustic laboratory measurements. In the proposed experimental setup, the simply supported boundary condition will be achieved by rigidly attaching the plate edges to thin vertical supports as in [6, 7, 11, 10, 12] but using gluing instead of screwing which greatly simplifies the implementation compared to other proposals. Special emphasis is put on providing precise technical guidelines to setup such a panel in practice, so that this laboratory tool can be reproduced, used and improved by the research community.

The theoretical background of the problem is first briefly recalled in Section 2. A design parameter for the plate edges supports to obtain adequate boundary conditions is then suggested and applied to the considered panel in Section 3. Detailed technical guidelines are given in Section 4, and illustrated with an assembly plan and mounting instructions. Apart from several already published works that made use of the described panel [14, 15, 16, 17], three additional application cases of the proposed panel and experimental validations are reported in Section 5 to provide an exhaustive overview of possible applications of this laboratory tool. The three presented cases concern (1) the measurement of the unbaffled panel response under a point mechanical excitation, (2) the measurement of the baffled panel response in a coupled rooms arrangement (i.e. under a Diffuse Acoustic Field excitation) and (3) the experimental validation of a coupled electrodynamic actuator - unbaffled plate model for active vibration control. Note that another application of interest would be as a teaching support as in Barnard [9], but such a possibility is not illustrated here.

2. Theoretical background

Figure 2a illustrates the problem under study. For a homogeneous and isotropic rectangular plate of length L_x and width L_y, and with a thickness h considered small compared to L_x and L_y so that only the transverse deflection $w(x, y; \omega)$ is considered (thin panel hypothesis), the free vibration equation for small harmonic displacements can be written

$$\tilde{D}\left(\frac{\partial^2}{\partial x^2}+\frac{\partial^2}{\partial y^2}\right)^2 w(x,y;\omega)-\rho h\omega^2 w(x,y;\omega)=0, \quad (1)$$

where ρ is the mass density of the plate, ω the angular frequency and $\tilde{D}$ the complex bending stiffness ($\tilde{D} = \tilde{E}h^3/12(1-\nu^2)$, with $\tilde{E}$ the complex Young's modulus including the structural damping factor η so that $\tilde{E} = E(1+\mathrm{j}\eta)$, and ν the Poisson's ratio). Achieving ideal simply supported conditions implies supporting a plane and thin structure, for which any edge can rotate freely while being restricted from out-of-plane displacements. These two conditions imply that bending moments and transverse displacements are zero on the plate boundaries. In this case, the eigenfrequencies $\tilde{\omega}_{mn}$ and eigenfunctions ϕ_{mn}, solutions of Equation (1) take simple closed-form expressions

$$\tilde{\omega}_{mn}=\sqrt{\frac{\tilde{D}}{\rho h}}\left[\left(\frac{m\pi}{L_x}\right)^2+\left(\frac{n\pi}{L_y}\right)^2\right], \quad (2)$$

and

$$\phi_{mn}(x, y) = \sin\left(\frac{m\pi x}{L_x}\right)\sin\left(\frac{n\pi y}{L_y}\right), \tag{3}$$

with m, n non-zero, strictly positive integers.

The displacement response of the plate at any (x, y) location is given by the following modal expansion

$$w(x, y; \omega) = \sum_{m=1}^{\infty}\sum_{n=1}^{\infty} q_{mn}(\omega)\,\phi_{mn}(x, y), \tag{4}$$

where $q_{mn}(\omega)$ is the complex modal amplitude which for a given modal force F_{mn} (depending on the nature of the plate's excitation) can be written

$$q_{mn}(\omega) = \frac{1}{\rho h L_x L_y}\frac{F_{mn}}{\tilde{\omega}_{mn}^2 - \omega^2}. \tag{5}$$

3. Simulations for approaching actual boundary conditions of a simply-supported plate

The accurate modeling of the boundary conditions applied along the edges of a structure as their practical implementation share common difficulties. Such boundary conditions are generally modeled using a rotational spring of stiffness k_r and a linear spring of stiffness k_f (see Figure 2b). Unlike ideal simply supported boundary conditions that imply a null rotational stiffness and an infinite transversal stiffness (i.e. $k_r = 0$ and $k_f = +\infty$), realistic simply supported boundary conditions are usually achieved with a small but finite rotational stiffness, and a large but finite transverse stiffness (a small amount of stiffness restrains the edges rotation, and a small but non-zero movement is allowed in the z-axis). Joga Rao and Lakshmi Kantham [18] studied the variation of the three first vibration modal frequencies of a square plate having uniform but variable slope restraints along all edges.

Bapat *et al.* studied the simulation of classical edge conditions [19] (clamped or simply-supported) by defining adequate values of flexibility in simulations that could be representative of either infinite or zero flexibility (in their work, flexibility was prefered to stiffness). These previously published results were used to propose a theoretical basis for experimentally achieving these specific boundary conditions [20], but no experimental validation was given. On their side, Warburton and Edney [21] numerically studied the variation of the fundamental frequency of plates with different aspect ratios and boundary conditions (including a simply-supported plate) using dimensionless rotational and translational restraints. The reader interested in further readings concerning such simulation works can refer to the bibliography given in [19, 21], and also to pages 117–123 in Leissa's book [2] concerning plates having continuous simply supported edge conditions.

As stated in the introduction, the simply supported boundary condition will be achieved here by rigidly attaching the plate's edges to thin vertical supports (see Figure 2c) as in [6, 7, 10] using gluing instead of screwing. The supports, or shims, that will now be called 'blades' throughout the paper, should be flexible enough to provide a small but finite rotational stiffness, but also rigid enough to support the panel's weight and provide sufficient translational restraint. As illustrated in Figure 2a, the structure under consideration is a plane panel with dimensions ($L_x \times L_y \times h$) and Young's modulus E. The dimensions of the vertical blades are ($L_b \times l_b \times h_b$), and Young's modulus E_b (see Figure 2c). As in [2, 7] and at a given frequency, the rotation stiffness can be approximated by an equivalent rotational spring constant per unit length for the blades named k_r^b,

$$k_r^b = \frac{E_b h_b^3}{12 l_b}. \tag{6}$$

A coefficient k_r^p may also be defined for the panel to be supported,

$$k_r^p = \frac{E h^3}{12 L_x}. \tag{7}$$

As proposed by Champoux [7], a simple and necessary condition for approaching simply supported boundary conditions would be $k_r^b < k_r^p$. In order to better predict the error on the plate eigenfrequencies induced by imperfect boundary conditions regarding to perfect simply supported boundary conditions, a criterion based on the ratio of these two coefficients is proposed and using a similar material for both panel and blades so that their Young's modulus are identical, that is

$$\frac{k_r^b}{k_r^p} = \frac{h_b^3 L_x}{h^3 l_b}. \tag{8}$$

This ratio will be used to relate frequency shift of eigenfrequencies when the height and thickness of the supporting blades are varied for fixed dimensions of the plate. Since an upper limit value of this ratio will be then defined in the following, only the length L_x of the panel is considered for calculations (since for a given value of the ratio k_r^b/k_r^p calculated with L_x and set as an upper bound, the criterion will be implicitly satisfied for L_y if $L_x > L_y$). Whatever the height and thickness of the blades, they will be considered to be stiff enough to prevent any in-plane motion of the plate edges, but flexible enough to allow a variable rotation (depending on chosen height and thickness). Table I gives the properties of the considered panel for both numerical simulations and experiments.

A finite element model is used to analyze the influence of blades dimensions on the computed eigenfrequencies of the plate. The data, computed with Comsol Multiphysics®, were obtained by varying the height or thickness of the vertical blades while keeping all other quantities constant. The modal solver was used, and the panel was meshed using the physics-controlled meshing tool provided (with a minimum element size of 1.93 mm and a maximum element size of 26.5 mm). Note that in the simulation model, the connections between blades and the

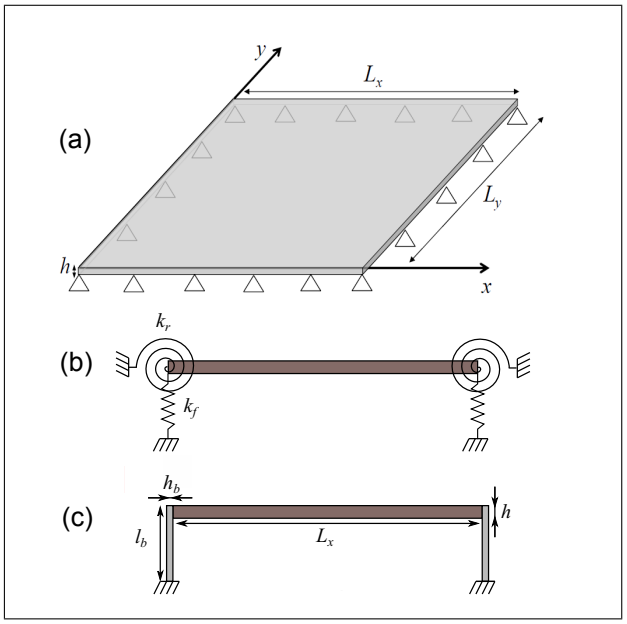

Figure 2. (a) General sketch of a panel of length L_x and width L_y simply supported along its edges - (b) Sideview of the panel with theoretical elastic boundary conditions illustrated - (c) Sideview of the panel with experimental boundary supports.

Table I. Properties of the simply supported aluminium panel.

Parameter (*Symbol*), Unit	Value
Young's modulus (E), GPa	70
Length (L_x), m	0.48
Width (L_y), m	0.42
Thickness (h), mm	3.19
Mass density (ρ), kg/m^3	2740
Bending stiffness (D), N·m	210.5
Poisson's ratio (ν)	0.3
Structural loss factor (η)	0.004

plane panel are supposed to be rigid and the clamping of the blades on the frame is supposed to be perfect, whereas in practice these conditions will not be perfectly fulfilled and both imprecisions will potentially introduces small amount of flexibility or rigidity that can not be taken into account at this step.

For each couple of height and thickness values, and a given (m, n) mode, the simulated natural frequency was compared to the theoretical one, and the corresponding percentage deviation was calculated (as in Ochs [6], it is here defined by 100 times the actual frequency difference divided by the theoretical one). As the plate's fundamental mode frequency (mode $(1, 1)$) was shown to be the most sensitive to changes in boundary conditions [19, 7, 21], the following results mainly focus on this eigenfrequency (from Equation (2), that is $f_{11} = \omega_{11}/2\pi = 77.03$ Hz).

Figures 3a,c show the effect of the blade height variation (for two fixed thicknesses) on the ratio k_r^b/k_r^p and on the percentage deviation on f_{11}, respectively. In a same manner, Figures 3b,d show the effect of the blade thickness variation (for two fixed heights) on the ratio k_r^b/k_r^p and on the percentage deviation on f_{11}, respectively. From

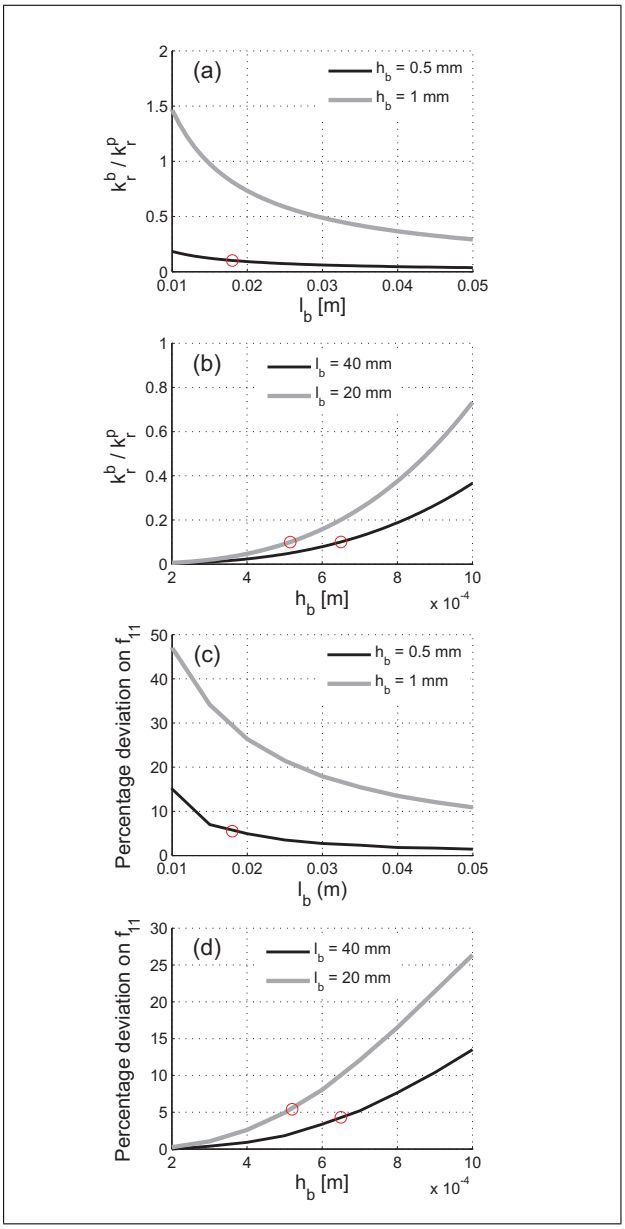

Figure 3. (a) Value of the ratio k_r^b/k_r^p when varying blade height for two fixed thicknesses - (b) Value of the ratio k_r^b/k_r^p when varying blade thickness for two fixed heights - (c) Percentage deviation on mode (1,1) frequency when varying blade height for two fixed thicknesses - (d) Percentage deviation on mode (1,1) frequency when varying blade thickness for two fixed heights / The red dots indicate the values of h_b, l_b for which the ratio k_r^b/k_r^p equals 0.1 and corresponding percentage deviation on f_{11}.

these figures, the values of the ratio k_r^b/k_r^p nearly vary as the percentage deviation on the frequency of mode $(1, 1)$. Equation (8) can be therefore useful for predicting the frequency shift when simply supported conditions are experimentally implemented. In practical terms, if a maximum frequency deviation $\%\Delta f$ of approximately 5% compared to ideal simply supported conditions is targeted on the first natural frequency of the plate, it can be deduced from the corresponding red dots plotted in Figures 3a-d that

- If the thickness h_b is set to 0.5 mm, then the blade's height l_b should be equal or larger than 18 mm.

Table II. Theoretical eigenfrequencies and calculated eigenfrequencies for the chosen blades dimensions, and corresponding percentage deviation on the ten first modes eigenfrequencies. Theoretical frequency: Real part of Equation (2) in Hz. Calculated frequency: $l_b = 2\,\text{cm}$, $h_b = 0.5\,\text{mm}$, [Hz].

(m,n) indices of considered mode	(1,1)	(2,1)	(1,2)	(2,2)	(3,1)	(1,3)	(3,2)	(2,3)	(4,1)	(3,3)
Theoretical frequency	77	177.3	207.9	304.1	344.3	426.1	475.2	526.3	578.1	693.3
Calculated frequency	80.8	180.8	211.7	311.3	347.5	429.6	477.6	528.9	580.8	694.6
Percentage frequency deviation	3.9	2	1.8	1	0.9	0.8	0.5	0.5	0.5	0.2

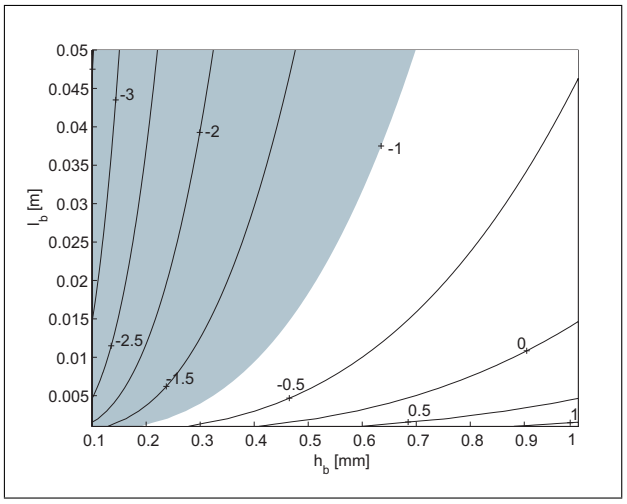

Figure 4. Mapping of $\log_{10}(k_r^b/k_r^p)$ for different (h_b, l_b) pairs of values - the white area highlights the (h_b, l_b) values for which the condition $\log_{10}(k_r^b/k_r^p) \leq -1$ is not fulfilled.

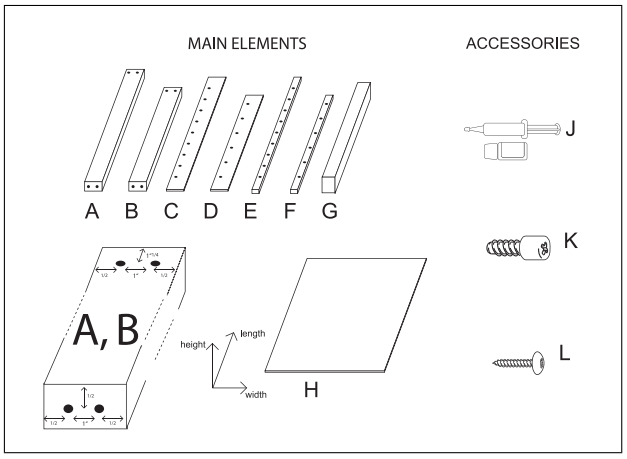

Figure 5. Simply supported panel schematic parts list (see description parts list in Table III).

- Conversely, if the blade's height l_b is set to 20 mm, then the blade's thickness has to be equal or lower than 0.5 mm.
- If the thickness h_b is set to 1 mm, then a maximum possible blade's height l_b of 50 mm will not allow reaching the desired frequency precision.
- The following simple empirical condition can be followed, $\%\Delta f \leq 5\% \quad \Leftrightarrow \quad k_r^b/k_r^p \leq 0.1$.

The ratio k_r^b/k_r^p could be linked to an objective upon frequency precision and be used as a design parameter to define adequate couples of height and thickness ((l_b, h_b) values) for the blades supporting a given panel. Such couples of values may be defined using a mapping as given in Figure 4, where the logarithm base 10 of the ratio k_r^b/k_r^p is calculated and plotted for various heights and thicknesses of the blades. For a target frequency precision of 5%, following the line of constant value $\log_{10}(k_r^b/k_r^p) = -1$ might help to take into account technical constraints. As an example, if only a thickness of 0.6 mm was available for construction, the blades height should now reach approximately 30 mm instead of previously 20 mm for a thickness of 0.5 mm.

Table II reports the theoretical and calculated eigenfrequencies for the ten first vibration modes (for given blades dimensions corresponding to the finally constructed panel). The higher percentage deviation is seen for mode $(1, 1)$ with a value of 3.9%, and is equal or lower than 2% for the nine other considered modes, and confirms the fact that the first vibration mode might be used to define a higher bound for frequency precision (that should then be reached for all the other vibration modes). Warburton and Edney [21] also noticed that the percentage change in terms of frequency tended to be smaller for higher modes compared to the fundamental one.

4. Experimental construction of panel

This section describes how several panels were constructed using the panel and blades dimensions considered in previous section. Figure 5 first schematically describes the main elements and accessories needed, and their precise descriptions and additional technical details are provided in Table III. It is precised that steel is chosen for the frame partially for reasons of cost, but mainly to ensure a high '*panel-and-edges to frame*' mass ratio so that the frame nearly behaves as a rigid and massive foundation from the panel's point of view. Using the materials and dimensions given in Table III, a mass ratio of approximately 0.09 is finally obtained (with a weight of 20.7 kg for the frame, and 1.8 kg for the panel and edges).

Figure 6 then gives visual instructions for assembly, which are to follow from left to right and top to bottom. Some additional remarks to this assembly plan are given below,

- As stated in Table III, the wedges role is to support the panel while being glued. They can be designed in various ways, but must be able to globally support the panel so that it will be flush mounted along all edges when

Table III. Parts list (see corresponding sketches in Figure 5).

Part number (quantity)	Description (material)	Dimensions (length by width by height) in inches [in cm, round]	Technical details (see Figure 5 for drawings)
A (x 2)	Frame longitudinal bar (steel)	**20 1/2 × 2 × 1** [52 × 5 × 2.5]	2 tapped holes at the bottom (part B mouting) 2 drilled holes at the top (see details in Figure 5) 9 equidistant tapped holes spaced by 2 in. [5 cm] (part C mounting)
B (x 2)	Frame transversal bar (steel)	**18 1/8 × 2 × 1** [46 × 5 × 2.5]	2 tapped holes at the bottom (part A mounting) 2 drilled holes at the top (see details in Figure 5) 6 equidistant tapped holes spaced by 2 1/4 in. [5.7 cm] (part D mounting)
C (x 2)	Longitudinal blade (aluminium)	**18 7/8 × 1 3/8 × 1/20** [48 × 3.5 × 0.05]	9 equidistant holes spaced by 2 in. [5 cm] 1/4 in. from left edge, 1/4 in. width [0.7 cm]
D (x 2)	Transversal blade (aluminium)	**16 1/2 × 1 3/8 × 1/20** [41.9 × 3.5 × 0.05]	6 equidistant holes spaced by 2 1/4 in. [5.7 cm] 1/4 in. from left edge, 1/4 in. width [0.7 cm]
E (x 2)	Longitudinal retainer bar (steel)	**17 1/2 × 1/2 × 1/4** [44.5 × 1.3 × 0.7]	9 equidistant holes spaced by 2 in. [5 cm] centered along width, 5/32 in. width [0.4 cm]
F (x 2)	Transversal retainer bar (steel)	**15 × 1/2 × 1/4** [38.1 × 1.3 × 0.7]	6 equidistant holes spaced by 2 1/4 in. [5.7 cm] centered along width, 5/32 in. width [0.4 cm]
G (x 2)	Assembly wedge (Block of wood, plastic, steel)		These wedges will help the correct positioning of the panel while gluing
H (x 1)	Panel (aluminium)	**19 × 16 1/2 × 1/8** [48 × 42 × 0.32]	
J (x 1)	Two-component glue (-)		Loctite 330 with 7387, activator is suggested
K (x 8)	Socket head partial thread (steel)		2 in. length 1 1/2 in. thread length, 5/16 in. width
L (x 30)	Socket head full thread (steel)		7/8 in. length 5/32 in. width

glued to the blades. These wedges will also prevent any possible bending of the panel.

- At the two gluing steps along length and width, and just after screws have been tighten to enclose the panel, it is strongly advised that an additional holding and clamping system is used to ensure homogeneous gluing along the panel edges or prevent sliding of the panel before gluing is complete. Some time should be allowed to pass between the two gluing steps (i.e. one after the other, not the two at the same time).
- A two-step (or two component) adhesive is suggested and preferred to instant adhesives to allow having some time to tighten screws and setup an additional holding system as suggested. In any case, an adhesive with high viscosity should be used (to avoid glue leaks along the blades while adhesive dries), with minimal shear and tensile strength suggested values of both 15 N/mm^2 (usually indicated in technical data sheets). Two-step adhesives usually provide such strength values with also high viscosity.
- After each gluing step, it is advised to follow drying times indicated for the chosen two-component glue.
- If the blades slightly exceed the panel surface after gluing is complete (i.e. a small burr), it is advised not deburring it since it could unglue the assembly.
- Parts A and B are designed to have their length slightly exceeding at each panel corner, which is made to compensate for the K bolts head height.
- The sides of part H should be machined so as to present a smooth and plane surface for gluing (the machined sides surface should be perpendicular to the panel surface).
- Removable supports or anchors should be ideally added at the panel base when mounted in a vertical direction (as in Figure 7) to improve stability of the panel (and prevent any movement or even fall).

Figures 7a-d show differents views of the panel after mounting. Note that after this step, the 'panel-and-blades' part can be easily disassembled and reassembled from the frame. This possibility has been often used to facilitate piezolectric actuators mounting [14] as an example, or to replace a damaged panel.

All the elements dimensions given here stand for setting up a similar panel than the one used in previous studies [14, 15, 16, 17] and in the present paper. Other dimensions

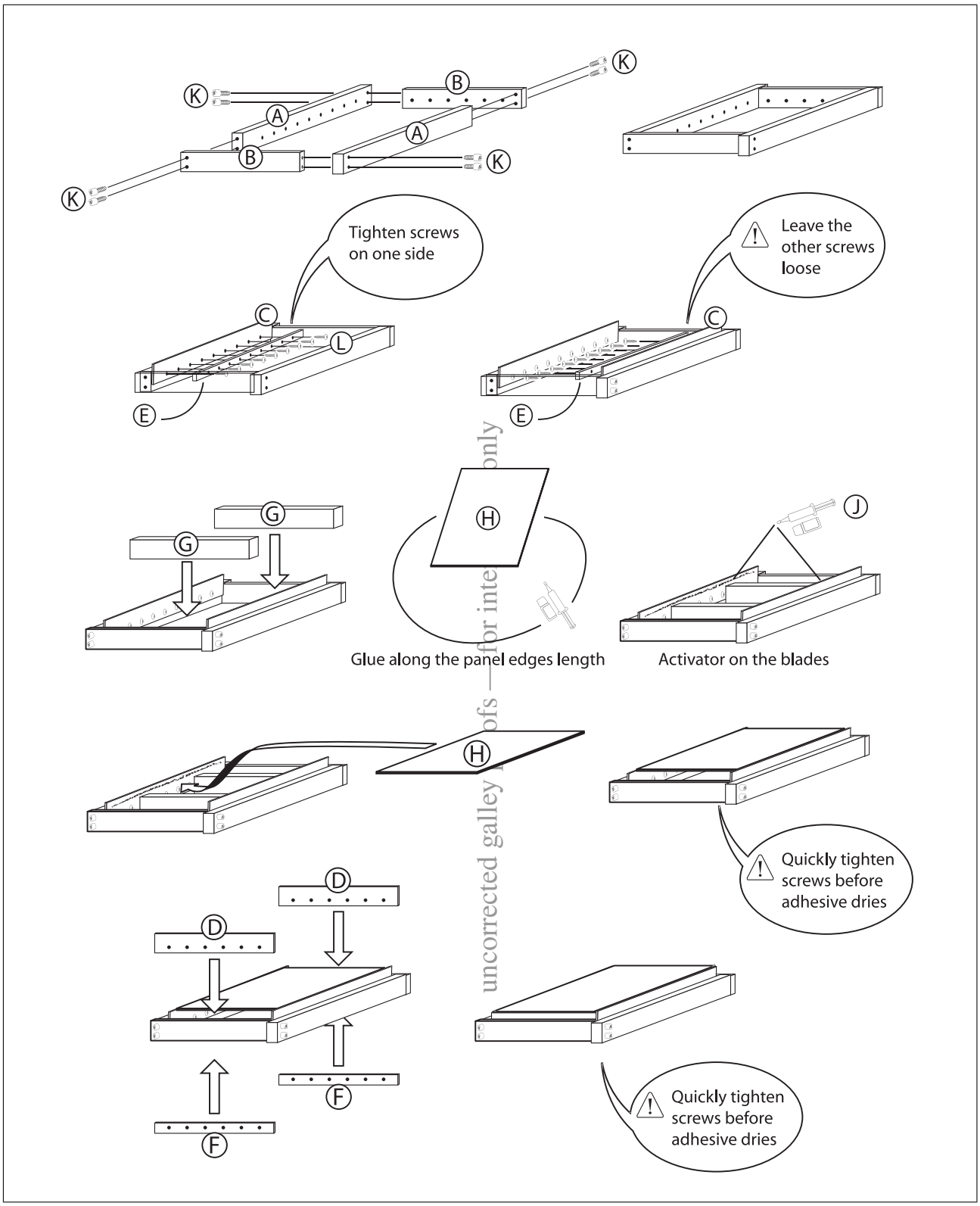

Figure 6. Assembly plan (to be read from left to right and top to bottom).

and technical details could be suitable to reproduce adequate simply-supported boundary conditions, but should be ideally validated either by simulations as described in previous section or by the proposed empirical approach using the ratio k_r^b/k_r^p. A way to realize avatar panels would be to rely on the similitude concept [22, 23], and build panels (and frame and blades) for which the dimensions are simply similar to those of the initial panel (i.e. all the dimensions of the new panel-blades-frame assembly should be linearly scaled by the same factor to the dimensions of

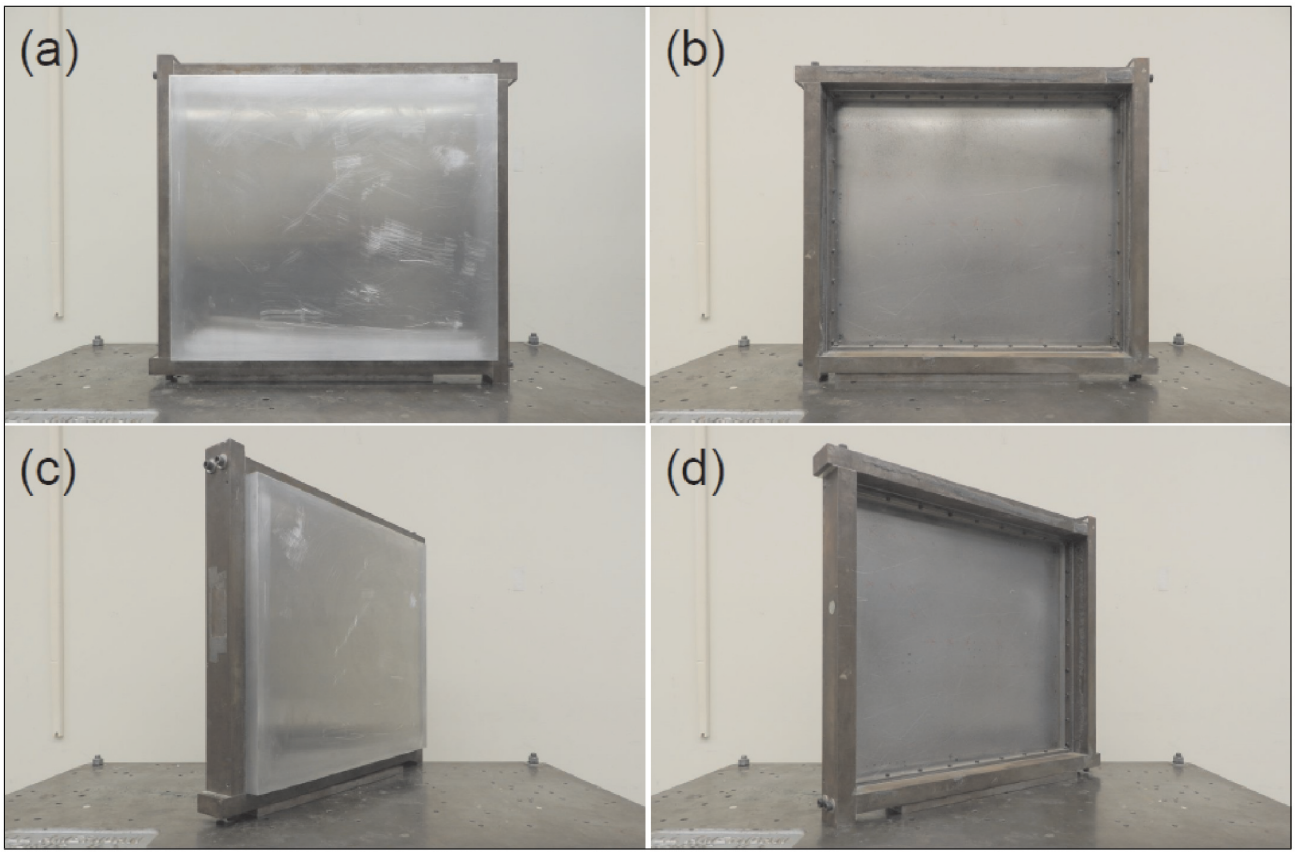

Figure 7. Differents views of the panel after mounting; (a) Front view; (b) Rear view; (c) Front view with a visual angle of approximately 30 degrees; (d) Rear view with a visual angle of approximately 30 degrees.

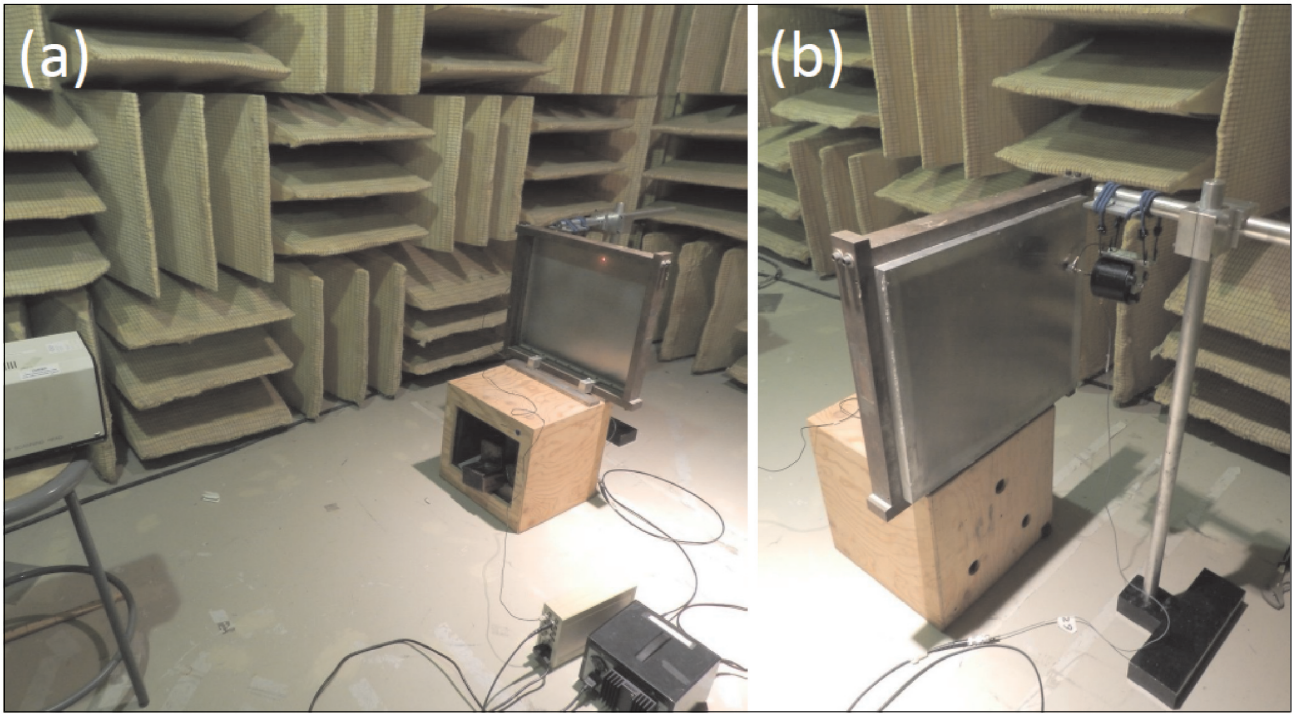

Figure 8. Experimental setup showing the unbaffled panel on a simple weighted wood stand in a hemi-anechoic room; (a) Panel seen from the LDV measurement side; (b) Shaker excitation on the other side of the panel.

the one presented here). Note finally that it was observed when disassembling/reassembling the panel on the frame that a firm and uniform clamping of the blades to the steel frame was important to reach the desired boundary condi-

tions, so that a comparable linear density of screws to the one used here should be ideally used.

5. Results of three different experiments conducted on the same panel

5.1. Application case 1: Panel vibratory response under a mechanical excitation

This section describes experiments made on the panel using a point mechanical excitation and a measurement of the transverse velocity of the panel. An electrodynamic shaker (Brüel&Kjær 4810) was mounted to the panel via a stinger and a force transducer (PCB 208C03) at a position $x = 0.06\,\mathrm{m}$ and $y = 0.30\,\mathrm{m}$. The transverse velocity of the panel was measured on a regular grid (27×23 points) over the plate surface using a Polytec scanning Laser Doppler Vibrometer (LDV), for a white noise input of the shaker in the $50 - 2000\,\mathrm{Hz}$ range. An average structural loss factor $\eta = 0.004$ was experimentally evaluated using the $-3\,\mathrm{dB}$ bandwidth method on the first few structural resonances of the panel, and supposed to be frequency independent. For such a small loss factor, it was assumed that the resonant response of the panel under mechanical excitation only include the corresponding vibration mode. The operational mode shapes identified at each resonance (i.e. peak) frequency were also considered identical to plate mode shapes.

Figures 8a,b illustrate the experimental setup. Note that a very similar measurement setup with the same panel but baffled can be found in [15, 16, 17], for its response measurement under point mechanical and acoustic excitations.

The theoretical mobility function (vibration velocity upon force) is calculated at the excitation point by using the derivative of Equation (4) for a unit force input (mode orders up to 50 in the x and y directions were used). The experimental mobility function at the excitation point was extracted from the LDV measurements. Figure 9 shows the comparison of the experimental and theoretical mobility functions. The agreement between analytical and experimental results is very satisfactory up to 1.5 kHz. Table IV confirms the good agreement between theoretical and measured eigenfrequencies. At the exception of the fundamental mode for which frequency deviation exceed the 5% limit (such sensivity of this mode was identified with predictions in Section 3 and by other researchers [19, 21]), the obtained experimental frequency deviations on the nine following modes closely follow the theoretical predictions reported in Table II. Similar results were reported in [15, 16, 17]. As an evidence, some measurements uncertainties could explain the percentage difference, such as an imperfect knowledge of the physical parameters (elastic modulus) and the small mass and stiffness added by the shaker stinger and force sensor (that were not taken into account here).

The theoretical mode shapes or eigenfunctions (see Equation 3) of four vibration modes [$(1,1)$, $(2,1)$, $(3,2)$ and $(3,3)$] are compared to the operational mode shapes

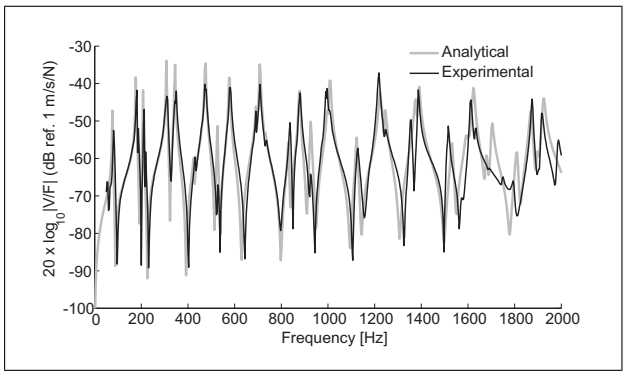

Figure 9. Comparison of analytical and measured mobility function (transverse velocity divided by force) at the excitation point - Analytical mobility is indicated by the thick gray line, while the experimental mobility is indicated by a thin black line.

in Figures 10a-h. The data used for plotting the operational mode shape were the plate displacement response to a unitary force input of the shaker at each considered experimental resonance frequency, that were then normalized to have a maximum equal to unity (as for theoretical mode shapes). Additional zero displacement points were also imposed along panel edges that were excluded from the measurements (finally leading to a regular grid of 29×25 points). As for the theoretical and experimental eigenfrequencies (see Table IV), the agreement between theoretical and experimental mode shapes is very satisfactory.

5.2. Application case 2: Panel Transmission Loss under a Diffuse Acoustic Field

Figure 11a illustrates the typical setup of a panel for its Transmission Loss (TL) measurement using coupled rooms. Figures 11b,c show pictures of the panel installed in the coupled rooms at Groupe d'Acoustique de l'Université de Sherbrooke from the anechoic room side and from the reverberant room side, respectively. Regarding the mounting conditions, the panel was first mounted in the existing niche and a plywood frame on $1/2$ in. thick was set around the panel so that both the panel and its baffle were nearly flush mounted in the reverberant room. A small gap of 1 mm was left along all the edges of the panel and filled with silicone seal to ensure acoustic insulation and mechanical decoupling from the baffle. A double wall structure was then built around the panel to prevent direct and indirect (flanking) acoustic leaks. It was constituted of the plywood panel previously cited, on which were fixed 3 vertical 2×4 in. lumbers and the 4 in. depth spaces created were filled with two layers of 2.75 in. glass wool. Finally, $3/4$ in. thick gypsum board was used to close the cavities, and the niche partitions and the steel edges of the panel were covered with an acoustic insulating material composed of a polyurethane foam and a viscoelastic layer (see Figure 11b).

A Diffuse Acoustic Field (DAF) excitation was generated in the reverberant room using one low and mid frequencies speaker positioned close to one of the opposite

Table IV. Theoretical and experimental eigenfrequencies for the ten first modes, and corresponding percentage deviation.

(m,n) indices of considered mode	(1,1)	(2,1)	(1,2)	(2,2)	(3,1)	(1,3)	(3,2)	(2,3)	(4,1)	(3,3)
Theoretical frequency (Real part of Equation (2)) [Hz]	77	177.3	207.9	304.1	344.3	426.1	475.2	526.3	578.1	693.3
Measured frequency at response peak [Hz]	82.1	181.3	212.5	307.8	348.4	431.3	478.1	530.6	584.4	696.9
Percentage frequency deviation %	6.6	2.3	2.2	1.2	1.2	1.2	0.6	0.8	1.1	0.5

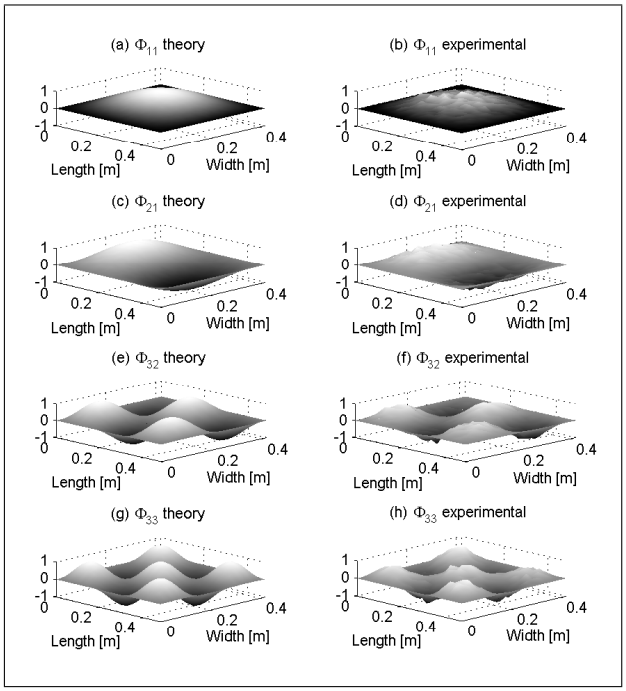

Figure 10. (a) Theoretical mode shape ϕ_{11} for mode $(1,1)$; (b) Operational mode shape ϕ_{11} for mode $(1,1)$; (c) Theoretical mode shape ϕ_{21} for mode $(2,1)$; (d) Operational mode shape ϕ_{21} for mode $(2,1)$; (e) Theoretical mode shape ϕ_{32} for mode $(3,2)$; (f) Operational mode shape ϕ_{32} for mode $(3,2)$; (g) Theoretical mode shape ϕ_{33} for mode $(3,3)$; (h) Operational mode shape ϕ_{33} for mode $(3,3)$ – Theoretical mode shapes are calculated using Equation (3).

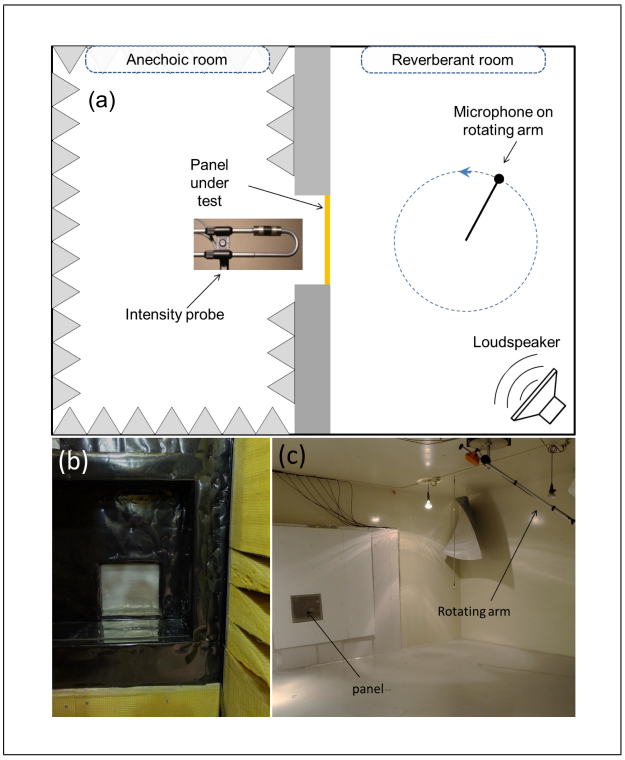

Figure 11. (a) Schematic description of typical panel mounting and setup for a TL measurement using coupled rooms; (b) View of the installed panel from the anechoic room side; (c) View of the installed panel from the reverberant room side.

corners of the room (compared to the panel's position). The space-averaged quadratic sound pressure in the reverberant room $< p^2_{RMS} >$ was obtained by rotating a microphone with at least a complete rotation of its supporting arm during the measurement, of 80 seconds duration (see Figures 11a-c). This allows estimating the incident acoustic power Π_{inc} on the panel of area S ($S = L_x \times L_y$), using the relation $\Pi_{inc} =< p^2_{RMS} > S/(4\rho_0 c_0)$ (with ρ_0 the air volume density and c_0 the speed of sound in air).

The radiated acoustic power Π_{rad} was estimated using the measured active acoustic normal intensity I_{rad}, integrated over S. A Brüel and Kjær intensity probe was used, composed of two half-inch microphones and a 12 mm spacer (this spacer size implies an upper frequency limit of 5 kHz for accurate sound intensity measurements). The panel area was manually scanned at a distance of 10 cm during the measurement so that a temporal and a spatial averaging were achieved, and the edges of the panel were excluded from the scan to avoid measuring potential acoustic leaks.

The Transmission Loss (TL) of the panel was finally calculated following

$$\mathrm{TL} = 10 \log_{10} \frac{\Pi_{inc}}{\Pi_{rad}}. \tag{9}$$

Numerical predictions of the TL were obtained using a finite element model[1]. The panel was modeled as a layer inserted in an infinite baffle separating two semi-infinite fluid domains, and meshed on 49 × 43 elements, leading to an element size of 1 cm ×1 cm which satisfies the common rule of six elements per wavelength up to a frequency

[1] NovaFEM ©Université de Sherbrooke and Mecanum Inc.

of nearly 6 kHz. The excitation was defined as a DAF with angles of incidence up to 90^o (summation of plane waves equally distributed between normal incidence case and this highest incidence angle).

Figures 12a-b present comparisons between simulation and measurements. From the results presented in Figure 12a with a linear frequency step of 2 Hz and on a linear frequency scale from 150 to 2000 Hz, the measured TL values are in good agreement with the simulations and all the TL gaps that correspond to structural resonances are well identified. Under a frequency of approximately 500 Hz, the measurement result nevertheless diverges from the simulated one, with either higher or lower values than those predicted. This is attributed to non-diffuse conditions in the reverberant room for frequencies lower than the Schroeder frequency f_S (which marks the transition from separated room modes to overlapping ones which results in an effectively diffuse acoustic field). In the present case, the volume V of the reverberant room is approximately 140 m^3 ($7.2 \times 6.5 \times 3$ m^3), and the corresponding theoretical Schroed er frequency f_S is 410 Hz ($f_S = 2000\sqrt{T/V}$, with a 60 dB mean reverberation time T taken equal to 5.9 seconds, and V the room volume [24]).

The results presented in Figure 12b in 1/12 octave bands and on a logarithmic frequency scale from 150 and 6000 Hz also confirm a good agreement between simulations and measurement from 300 to 6000 Hz. The divergence between simulated and experimental results below a frequency of approximately 350 Hz is highlighted. Note also that the coincidence frequency can be quite well identified (its theoretical value is denoted by a vertical arrow in Figure 12b). The coincidence phenomenon occurs when the speed of sound c_0 equals the plate bending wave speed c_f, and the corresponding specific frequency f_c can be calculated using

$$f_c = \frac{c_0^2}{2\pi}\sqrt{\frac{\rho h}{D}}. \tag{10}$$

For this thickness and $c_0 = 343$ m/s, the theoretical coincidence frequency f_c equals 3854 Hz.

5.3. Application case 3: Dynamic coupling with an inertial actuator for active control

The example below considers an electrodynamic inertial actuator mounted on the simply supported plate detailed in Section 2. Such actuators are commonly used to implement active control strategies for a wide range of structural control problems, usually associated with vibration sensors [4, 25, 26, 27]. When mounted on a flexible structure such as the plate modeled in Section 2, the presence of the actuator will lead to an increase in overall mass and a change in the local stiffness, that will inevitably alter the dynamic properties of the structure. Knowledge on how the structure and actuators attached thereto interact dynamically, based on both a model and a laboratory tool, can be helpful for evaluating the control performance, including robustness and stability.

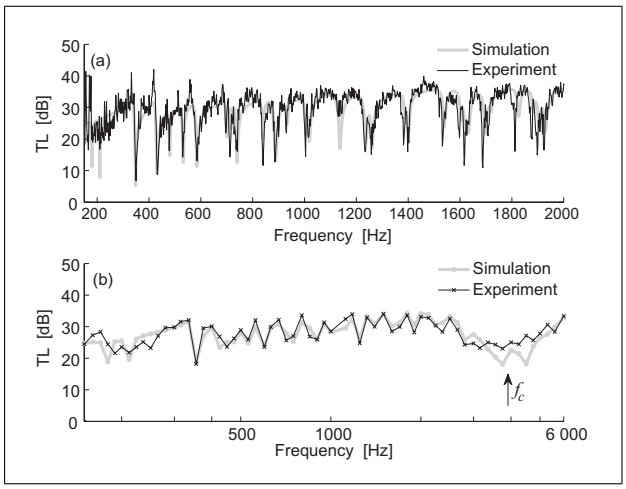

Figure 12. (a) Comparison of theoretical TL (thick gray line) and experimental TL (thin black line) results on a linear frequency axis from 150 to 2000 Hz; (b) Comparison of theoretical TL (thick gray line with circle markers) and experimental TL (thin black line with cross markers) in 1/12 octave-bands on a logarithmic frequency axis from 150 to 6000 Hz - the theoretical critical frequency f_c is indicated by a vertical arrow.

Table V. Physical parameters of the VISATON EX 60 S electrodynamic exciter.

Parameter	Notation	Value	Unit
Transduction coefficient	Bl	4.6	N A^{-1}
Dynamic mass	M_a	0.108	kg
Frame mass	M_f	0.0134	kg
Mechanical resistance	R_a	5.32	N s m^{-1}
Suspension stiffness	K_a	24 10^3	N m^{-1}
Natural frequency	f_n	75	Hz

Figure 13a-b illustrates the experimental setup used to investigate the dynamic interaction between the actuator and the plate, where the constant parameters Bl, M_a, R_a and K_a given in Figure 13b are the transduction coefficient, the dynamic mass, the mechanical resistance and the effective stiffness of the actuator, respectively, M_f is mass of the actuator frame, and R_e and L_e are the resistance and inductance of the moving coil transducer, respectively. Upon actuation using a current drive source as shown in Figure 13b, the open loop response function of the actuator at a given (x, y) position on the plate, defined as the ratio of the velocity v_s at the actuator base over the applied current i and expressed in m s^{-1} A^{-1}, can be derived as

$$G_i(\omega) = \frac{v_s}{i} = \frac{\mathrm{j}\omega M_a Bl\, Y(\omega)}{Z_{ma}(\omega) + \mathrm{j}\omega M_a\left(Z_{ms}(\omega) + \frac{M_f}{M_a} Z_{ma}(\omega)\right) Y(\omega)}, \tag{11}$$

where $Z_{ms}(\omega) = R_a + K_a/\mathrm{j}\omega$ is the mechanical impedance of the spring-dashpot mounting system, $Z_{ma}(\omega) = Z_{ms}(\omega) + \mathrm{j}\omega M_a$, and $Y(\omega) = v_s/f_s$ is the mobility function of the structure at the location of the actuator. $Y(\omega)$ can be

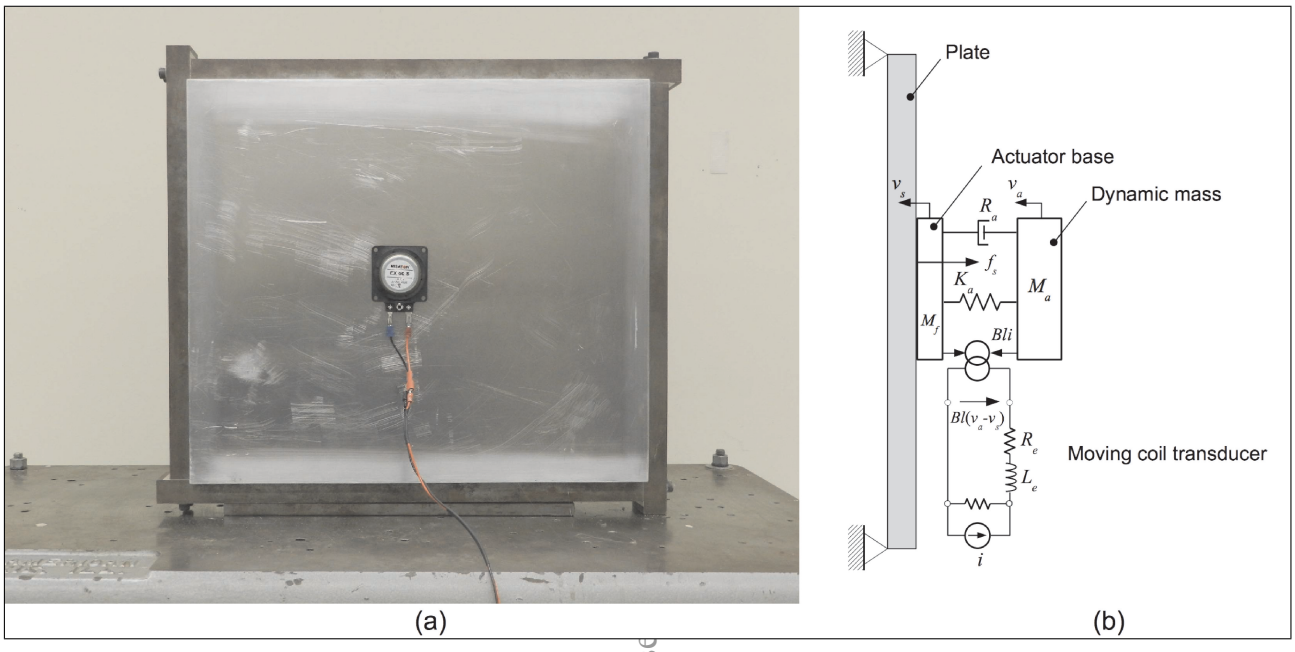

Figure 13. (a) Pictures showing the inertial actuator attached to the plate with a view to active vibration control; (b) Electro-mechanical model of the actuator connected to the plate, and driven using a current source (see Table V for the values of the indicated parameters).

derived using Equations (2)–(5), with v_s calculated as the displacement w multiplied by jω, and finally

$$Y(\omega) = -\mathrm{j}\omega \frac{1}{\rho h L_x L_y} \sum_{m=1}^{\infty} \sum_{n=1}^{\infty} \frac{\phi_{mn}^2(x,y)}{\omega_{mn}^2 - \omega^2}. \qquad (12)$$

More details on the lumped parameter model of the actuator can be found in [4, 27].

Figure 14 illustrates the open loop frequency response function v_s/i of the actuator near the center of the plate, where measured data (thin black line) were obtained using VibroMet 500V laser Doppler velocimeter (sensitivity 5 mV/(m s^{-1})) and computed data (thick gray line) are derived from Equation (11). As can be seen in Figure 14, theoretical and experimental results show good agreement in the frequency range of 0–2 kHz. Note that in this example the resonance frequency of the inertial actuator, at about 72 Hz, is very close to the first natural frequency of the plate, at about 77 Hz, which explains why the phase diagram exhibits strong variations below a value of approximately 80 Hz (it has been shown that the actuator natural frequency should be well below the first resonance of the structure to improve stability of the control for high control gain [26]).

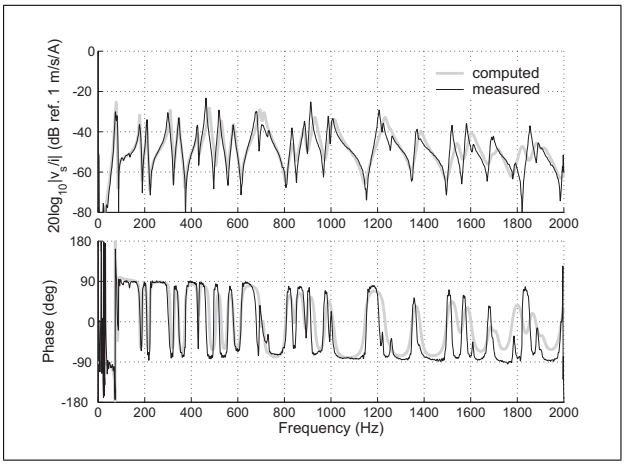

Figure 14. Bode plot of the open loop frequency response function of the actuator when attached near the center of the plate. Computed data are indicated by the thick gray line and measured data are indicated by a thin black line.

6. Conclusion

This paper described a technique for realizing representative simply supported boundary conditions on a panel and obtaining a functional experimental mean that can easily adapt to typical vibroacoustic laboratory measurements. A simple parameter to design blades that support a panel with given dimensions was first suggested and used in simulations for designing blades dimensions so as to reach a given frequency precision compared to theoretical eigenfrequencies for a simply supported panel, and was numerically validated using a finite element model. In order to ease the spread of this laboratory tool, precise technical guidelines were then given with an assembly plan so that it can be acquired, used and improved by the research community. Finally, three application cases were described to provide an exhaustive validation and to illustrate possible uses of this laboratory tool. For a frequency precision fixed here to 5%, the obtained experimental frequency deviations were shown to closely follow previous theoretical predictions at the exception of the fundamental vibration mode, which confirmed such sensitivity of this mode to imperfect boundary conditions as was identified by other

researchers. All the obtained experimental results in the three reported applications cases shown good agreement with analytical solutions and numerical predictions.

Acknowledgments

The authors are grateful fo all GAUS members that have contributed to, or used these panels for years (or will). First author especially thanks Patrick Levesque and Gabriel Laperle for their precious technical assistance, and beloved Nadia Zouaoui for her help on the visual instruction guide.

References

[1] A. W. Leissa: The free vibration of rectangular plates. J. Sound Vib. **31**(3) (1973) 257–293.

[2] A. W. Leissa: Vibration of plates. NASA SP-1960, 1969, Chap. 4, 41–159.

[3] E. G. Williams: Fourier Acoustics: Sound radiation and nearfield acoustical holography. Academic Press, San Diego, CA, USA, 1999. Chap. 2.14, 62–77.

[4] F. Fahy and P. Gardonio. Sound and structural vibration: radiation, transmission and response. 2nd edition. Academic Press, Oxford, UK, 2007. Chap. 2 and Chap. 9.

[5] G. Squicciarini, D. J. Thompson, R. Corradi: The effect of different combinations of boundary conditions on the average radiation efficiency of rectangular plates. J. Sound Vib. **333** (2014) 3931–3948.

[6] J. B. Ochs, J. C. Snowdon: Transmissibility across simply supported thin plates. I. Rectangular and square plates with and without damping layers. J. Acoust. Soc. Am. **58**(4) (1975) 832–840.

[7] Y. Champoux, S. Brunet, A. Berry: On the construction of a simply supported rectangular plate for noise and vibration studies. Experimental Techniques **20**(1) (1996) 24–26.

[8] W. H. Hoppmann II, J. Greenspon: An experimental device for obtaining elastic rotational constraints on the boundary of a plate. Proceedings of the 2nd U.S. National Congress of Applied Mechanic, University of Michigan, Ann Arbor, Michigan, June 14–18, 1954.

[9] A. R. Barnard, S. A. Hambric: Development of a set of structural acoustic teaching demonstrations using a simply-supported plate. Proceedings of the Noise-Con 2014 Conference, Fort Lauderdale, FL, USA, September 08–10, 2014.

[10] C. H. Hansen, S. D. Snyder: Active control of noise and vibration. E & FN Spon, London, UK, 1997. Chap. 11, 1136.

[11] J. Pan, S. D. Snyder, C. H. Hansen, C. R. Fuller: Active control of far-field sound radiated by a rectangular panel – A general analysis. J. Acoust. Soc. Am. **91**(4) (1992) 2056–2066.

[12] S. H. Yoon, P. A. Nelson: Estimation of acoustic source strength by inverse methods. Part II: Experimental investigation of methods for choosing regularization parameters. J. Sound Vib. **233**(4) (2000) 669–705.

[13] J. M. Minguez: An experimental investigation of how accurate, simply supported boundary conditions can be achieved in compression testing of panels. Experimental Mechanics **26**(3) (1986) 238–244.

[14] N. Quaegebeur, P. Micheau, A. Berry: Decentralized harmonic control of sound radiation and transmission by a plate using a virtual impedance approach. J. Acoust. Soc. Am. **125**(5) (2009) 2978–2986.

[15] O. Robin, A. Berry, S. Moreau: Experimental vibroacoustic testing of plane panels using synthesized random pressure fields. J. Acoust. Soc. Am. **135**(6) (2014) 3434–3445.

[16] A. Berry, O. Robin, F. Pierron: Identification of dynamic loading on a bending plate using the Virtual Fields Method. J. Sound Vib. **333**(26) (2014) 7151–7164.

[17] O. Robin, A. Berry, N. Atalla, S. A. Hambric, M. R. Shepherd: Experimental evidence of modal wavenumber relation to zeros in the wavenumber spectrum of a simply supported plate (L). J. Acoust. Soc. Am. **137**(5) (2015) 2978–2981.

[18] C. V. Joga Rao, C. Lakshmi Kantham: Natural frequencies of rectangular plates with edges elastically restrained against rotation. J. Aeronautical Sciences **12** (1957) 855-856.

[19] A. V. Bapat, N. Venkatramani, S. Suryanarayan: Simulation of classic edge conditions by finite elastic restraints in the vibration analysis of plates. J. Sound Vib. **120**(1) (1988) 127–140.

[20] A. V. Bapat, S. Suryanarayan: A theoretical basis for the experimental realization of boundary conditions in the vibration analysis of plates. J. Sound Vib. **163**(3) (1993) 463–478.

[21] G. W. Warburton, S. L. Edney: Vibrations of rectangular plates with elastically restrained edges. J. Sound Vib. **95**(4) (1984) 537–552.

[22] S. De Rosa, F. Franco, T. Polito: Structural similitudes for the dynamic response of plates and assemblies of plates. Mechanical systems and signal processing **25** (2011) 969-980.

[23] S. De Rosa, F. Franco, V. Meruane: Similitudes for the structural response of flexural plates. Proceedings of the Institution of Mechanical Engineers. Part C. Journal of Mechanical Engineering Science 1-15 (2015) In press.

[24] M. Schroeder: The 'Schroeder frequency' revisited. J. Acoust. Soc. Am. **99**(5) (1996) 3240–3241.

[25] S. J. Elliott, P. Gardonio, T. C. Sors, M. J. Brennan: Active vibroacoustic control with multiple local feedback loops. J. Acoust. Soc. Am. **111**(2) (2002) 908–915.

[26] S. J. Elliott, J. Rohlfing, P. Gardonio: Multifunctional design of inertially-actuated velocity feedback controllers. J. Acoust. Soc. Am. **131**(2) (2012) 1150–1157.

[27] R. Boulandet, A. Pelletier, P. Micheau, A. Berry: Active vibration control using self-sensing actuators: an experimental comparison of piezoelectric and electromagnetic technologies. Proceedings of the ASME 2014 International Mechanical Engineering Congress and Exposition - IMECE 2014, Montréal, Canada, November 14–20, 2014.